

Dynamic vehicle–bridge interaction under simultaneous vertical earthquake excitation

T. S. Paraskeva¹ · E. G. Dimitrakopoulos¹ · Q. Zeng¹

Received: 15 December 2015 / Accepted: 28 May 2016
© Springer Science+Business Media Dordrecht 2016

Abstract Traditionally, the seismic response analysis of a bridge does not account for the concurrent vehicle–bridge dynamic interaction. However, the behavior of a seismically excited bridge can jeopardize the safety of the vehicles running on it, even if the bridge itself remains undamaged. This study examines the seismic response of a vehicle–bridge interacting (VBI) system under vertical earthquake excitation, modelling the truck vehicles as rigid body assemblies. An application of the proposed scheme to a realistic case of (highway) bridge—(truck) vehicles shows that the earthquake ground motion and the road surface conditions are the main sources of excitation. The results show that the road surface conditions influence strongly the dynamics of the VBI system, even when the vertical component of the earthquake excitation is significant. Also, the study brings forward the influence of traffic parameters (namely the speed, the number and the distance between the running vehicles) and underlines the need to consider different positions of the vehicle/s (on the deck) during the earthquake shaking. Finally, it examines the tendency of the wheels of a truck vehicle to detach (jump) from the deck during the seismic response of the VBI system. Detachment tends to be more frequent as the road surface conditions deteriorate and/or the peak ground acceleration increases. However, detachment is a complicated phenomenon which depends also on many other ground motion and VBI system parameters and deserves further study.

Keywords Vehicle–bridge interaction · Truck modelling · Earthquake engineering · Seismic response · Bridges · Dynamic analysis · Wheel detachment

✉ T. S. Paraskeva
thparask@gmail.com

E. G. Dimitrakopoulos
iliask@ust.hk

Q. Zeng
qzeng@ust.hk

¹ Department of Civil and Environmental Engineering, Hong Kong University of Science and Technology, Clear Water Bay, Kowloon, Hong Kong

1 Introduction

A seismically vibrating bridge affects dramatically the safety of the running vehicles (Basoz and Kiremidjian 1998; Chang 2000). Drivers feel the seismically induced vibrations during earthquake shaking (Maruyama and Yamazaki 2002). As a consequence, traffic accidents could occur, even when the bridge itself remains undamaged, either owing to the difficulty of controlling the vehicles during the earthquake, and/or due to the driver's spontaneous over-reaction to the sudden, and without warning, earthquake vibration (Kawashima et al. 1989). The ever increasing traffic volume, due to the undergoing urbanization implies that the possibility of vehicles encountering an earthquake while crossing a bridge is also increasing. This underlines the growing need to investigate the seismic response of the interacting vehicle–bridge system, instead of focusing (solely) on the seismic behavior of the bridge.

Traditionally, the dynamics of moving vehicles and of earthquake excitation have been considered independently when analyzing the (seismic) response of bridges (e.g. Priestley et al. 1996; Kappos et al. 2012, 2013; and references therein). Characteristically, the existing seismic codes and guidelines worldwide (Japan Road Association 2002; CEN 1991; AASHTO 1996) account for the traffic action solely as an additional vertical live load/mass on the bridge. Taking a step forward, the recent study of Ghosh et al. (2013) deployed a framework for joint seismic and traffic-load fragility assessment for highway bridges. In a probabilistic approach, the stationary concentrated loads of a 3-axle truck were incorporated in the analyses, on various positions on the deck. That study resulted in seismic fragility curves for the bridge, including the effect of the traffic loading. Two recent large-scale seismic bridge shake tests examined the same problem. Wibowo et al. (2012) performed shake table seismic tests of a 2/5-scale model of a three-span bridge loaded with a series of (stationary) trucks. The experiments showed that the presence of the stationary trucks had a beneficial effect on the performance of the examined bridge for small amplitude motions, but this improvement diminished with increasing amplitude of shaking. Shaban et al. (2015) tested a 12-m long bridge of 20 tonnes, with and without, a stationary 1 ton urban motorcar. Again, the presence of the vehicle reduced the measured deck transverse acceleration and bearing displacements.

The seismic response of interacting vehicle–bridge systems has been analyzed in more detail for railway bridges and trains. Several studies (Kim and Kawatani 2006; Kim et al. 2011; He et al. 2011) verified that the seismic response of the bridge is reduced when the dynamics of the vehicles are properly simulated, whereas it is amplified when the vehicles are treated as additional vertical masses. Yang and Wu (2002) investigated the stability of train vehicles, stationary or moving, on bridges shaken by earthquakes. They stressed the significant effect of the vertical ground motion component on the stability of the train-rail bridge system. Further studies have been conducted by Matsumoto et al. (2004), Xia et al. (2006), Tanabe et al. (2008, 2011a, b), Yau (2010) and Du et al. (2012). Recently, the two last authors of the present paper proposed a scheme for the seismic response analysis of interacting (horizontally) curved railway bridges and trains (Zeng and Dimitrakopoulos 2016).

Further, vehicle-dynamics literature focuses on ride comfort and/or safety of running vehicles, without considering the interaction/coupling with a bridge. Uys et al. (2007) investigated the response of vehicles for various road profiles and vehicle speeds to determine the spring and damper settings that ensure optimal ride comfort. Els (2005) assessed the applicability of ride comfort standards, experimentally. Yang et al. (2009)

introduced an annoyance rate model and assessed it with experimental results. Maruyama and Yamazaki (2002) examined the effects of shaking to running vehicles and later conducted virtual tests using a driving simulator (Maruyama and Yamazaki 2004) to investigate the driver's reaction during an earthquake. They concluded that the strong ground shaking could affect the driver's response and trigger traffic accidents.

From the standpoint of urban resilience, there is a growing need to examine the seismic performance of the coupled vehicle–bridge system instead of focusing solely on the performance of the bridge. The present research is motivated by the need to elucidate how the seismic response of a bridge affects the safety and comfort of running vehicles. Specifically, this paper proposes a dynamic analysis approach for the seismic response of a vehicle–bridge interacting system, and examines a realistic (highway) bridge—(truck) vehicle case under the influence of seismic ground motions in the vertical direction.

2 Proposed analysis of the interacting vehicle–bridge system

The present paper offers a direct time-integration dynamic analysis approach of a vehicle–bridge interacting (VBI) system, under the simultaneous action of earthquake ground motions. As a first step, the study examines the response of the VBI system in, solely, the vertical direction. This is a limiting assumption, but it simplifies an already overcomplicated and multi-parametric problem and makes the analysis more economic in terms of computational cost. Hence, the simulation is two-dimensional (2D) along the vertical and the longitudinal direction of the bridge. The examined dynamical system consists of the vehicle subsystem and the bridge subsystem. The two subsystems are coupled through the contact forces between the vehicle wheels and the deck of the bridge. The study simulates the bridge with the finite element method and models the vehicle as a multibody assembly. The proposed analysis scheme derives from a previous work of Dimitrakopoulos and Zeng (2015), on vehicle–bridge interaction between trains and (horizontally) curved bridges, with the following changes: (1) the interaction model herein follows a different approach and results in modified equations of motion for the VBI system (compared to Dimitrakopoulos and Zeng 2015). Specifically, it calculates the contact forces based on the compliance of the tires and accounts for (the potential) detachment of the wheels from the deck. (2) The approach incorporates the simultaneous action of the vertical component of the earthquake ground motion, and (3) it is adjusted to truck vehicles travelling along the bridge.

2.1 Equations of motion of the interacting vehicle–bridge system

In general, the VBI analysis can be divided into the simulation of (1) the bridge, (2) the vehicle, and (3) the interaction between them (Dimitrakopoulos and Zeng 2015).

The finite element model of the bridge is built with commercial software (ANSYS 2007). Euler–Bernoulli beam elements (Cook 2007) are used, and a $\xi = 5\%$ damping ratio is assumed for the first 2 vertical modes of the bridge (see Fig. 1c). The stiffness matrix \mathbf{K}^B , the mass matrix \mathbf{M}^B and the Rayleigh damping matrix \mathbf{C}^B are then exported to an in-house MATLAB (MathWorks 2012) algorithm, developed and verified, previously (Dimitrakopoulos and Zeng 2015). The equations of motion for the bridge can be written in a general form as:

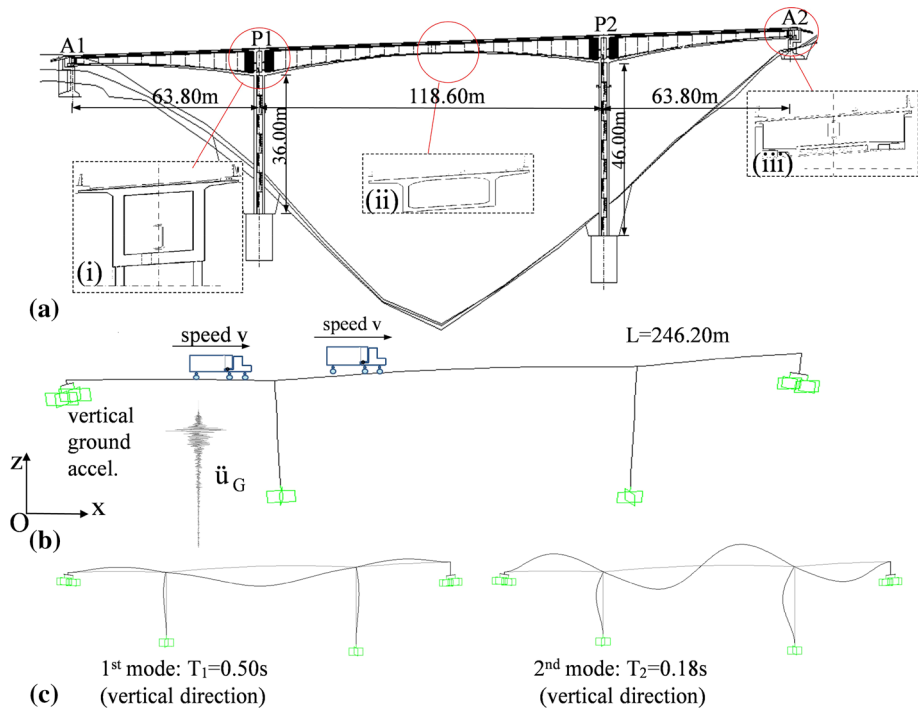


Fig. 1 **a** Layout of the bridge configuration, **b** the finite element model, and **c** the first two vertical modes of the bridge; *insets* in **(a)** show the deck sections (i) on top of the piers, (ii) in the middle of each span, and (iii) on the top of the abutments

$$\mathbf{M}^B \ddot{\mathbf{u}}^B + \mathbf{C}^B \dot{\mathbf{u}}^B + \mathbf{K}^B \mathbf{u}^B + \mathbf{W}^B \boldsymbol{\lambda} = \mathbf{F}^B \tag{1}$$

where the superscript $()^B$ denotes the bridge subsystem; \mathbf{u}^B is the bridge displacement vector; \mathbf{W}^B is the direction matrix of the contact forces for the bridge subsystem and $\boldsymbol{\lambda}$ is the vector of the coupling contact forces. \mathbf{F}^B is the vector of forces acting on the bridge including the earthquake ground motion, given as:

$$\mathbf{F}^B = -\ddot{\mathbf{u}}_G \boldsymbol{\delta}^B \mathbf{M}^B \tag{2}$$

where $\ddot{\mathbf{u}}_G$ is the ground acceleration at the base of the bridge (see Fig. 1) and $\boldsymbol{\delta}^B$ is a unit vector connecting the ground motion to the pertinent degrees of freedom (DOF) of the bridge.

Since the analysis is 2D, three DOFs are considered per node: two displacements with respect to the X-longitudinal and Z-vertical axis, and one rotation about Y axis (see Fig. 1).

Similarly, the equation of motion of the vehicle can be written as

$$\mathbf{M}^V \ddot{\mathbf{u}}^V + \mathbf{C}^V \dot{\mathbf{u}}^V + \mathbf{K}^V \mathbf{u}^V - \mathbf{W}^V \boldsymbol{\lambda} = \mathbf{F}^V \tag{3}$$

where the force vector \mathbf{F}^V , containing the gravity forces \mathbf{F}_G^V , and the earthquake inertia forces is given as:

$$\mathbf{F}^V = \mathbf{F}_G^V - \ddot{\mathbf{u}}_G \delta^V \mathbf{M}^V \tag{4}$$

Superscript $()^V$ denotes the vehicle subsystem; $\ddot{\mathbf{u}}^V$ is the acceleration vector; \mathbf{M}^V , \mathbf{C}^V and \mathbf{K}^V are the mass matrix, the damping matrix and the stiffness matrix of the vehicle, respectively; \mathbf{W}^V is the direction matrix of the contact forces. The latter can be defined by setting the DOFs of the wheels and the bridge elements involved in contact equal to unity.

The truck vehicle model is an assembly of rigid-bodies (i.e. the car body and the wheel sets) connected with springs and dashpots representing the suspension system (Cai and Chen 2004; Dimitrakopoulos and Zeng 2015). Figure 2 presents the two 2D vehicle models examined in the present study (see more details in Sect. 3.2). Since the focus is on the vertical response of the vehicle–bridge system, the simulation assigns 2 DOFs to each rigid body (subscript ‘rb’): the vertical displacement of the center of mass of the rigid body $Z_{v,rb}$, and the pitching rotation in x – z plane, $\theta_{v,rb}$. Each wheelset has only one DOF, the vertical displacement along the central line of the j axle, $Z_{a,j}$.

In summary, the displacement vector \mathbf{u}^V for the three- axle vehicle (i.e. the truck tractor with trailer) is:

$$\mathbf{u}^V = [Z_{v,1} \ \theta_{v,1} \ Z_{a,1} \ Z_{a,2} \ Z_{v,2} \ Z_{a,3}]^T \tag{5}$$

Similarly, the displacement vector for the five- axle vehicle (i.e. the truck tractor with two trailers) is:

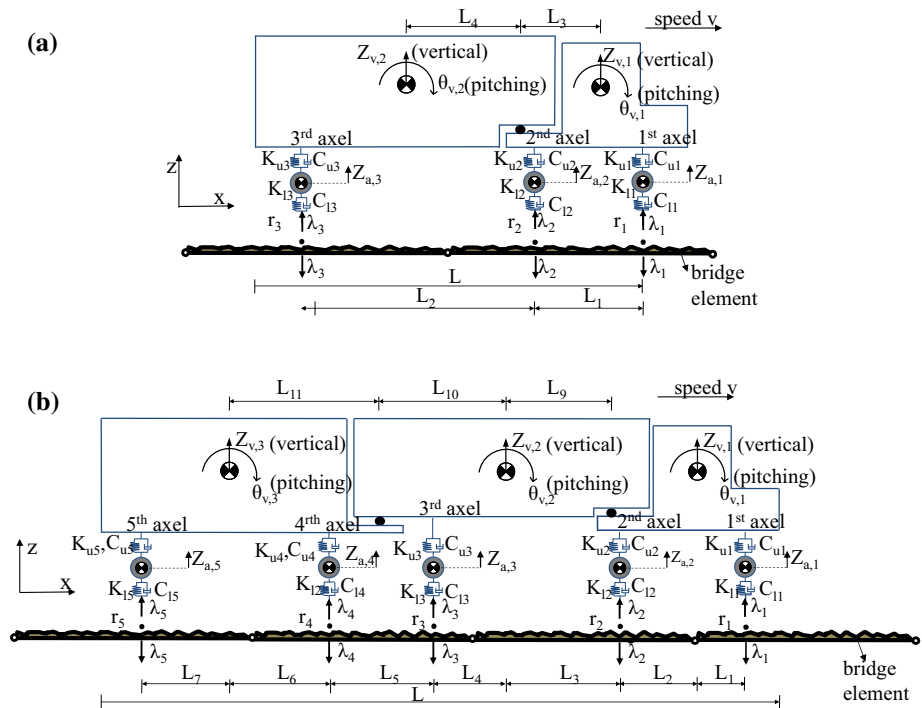


Fig. 2 The adopted 2D vehicle models: **a** a three-axle truck with one trailer; **b** a five-axle truck with two trailers

$$\mathbf{u}^V = [Z_{v,1} \ \theta_{v,1} \ Z_{a,1} \ Z_{a,2} \ Z_{v,2} \ Z_{a,3} \ Z_{v,3} \ Z_{a,4} \ Z_{a,5}]^T \tag{6}$$

With reference to the three-axle truck, note that the two truck rigid bodies are connected with a hinge (Fig. 2a) at distance L_3 from center of mass of the body 1, and L_4 from center of mass of the body 2, respectively. Thus, the pitching rotation of the second truck body, $\theta_{v,2}$ is a depended variable and can be evaluated as a function of the vertical displacement variables as:

$$\theta_{v,2} = \frac{Z_{v,2} - Z_{v,1} - \theta_{v,1}L_3}{L_4} \tag{7}$$

The pitching rotation of the second and third truck body, $\theta_{v,2}$ and $\theta_{v,3}$, respectively, for the five-axle truck, are calculated similarly.

The equations describing the motion of the bridge (Eq. 1) and the motion of the vehicle (Eq. 3) are coupled by the time-dependent contact forces λ (Fig. 2). Considering a single wheel at contact point j the coupling contact force can be expressed as:

$$\lambda_j = -K_{lj}g_j - C_{lj}\dot{g}_j \tag{8}$$

where K_{lj} and C_{lj} are the stiffness and damping coefficients of the wheel (derived from the compliance of the tire) at contact point j (see Table 1, and Wang et al. (2016); Zhang and Cai (2011); Yang et al. 2009) and g_j is the contact distance (relative displacement) between the wheel and the bridge element (as in Fig. 3) and \dot{g}_j is the corresponding relative velocity, given by

$$\begin{aligned} g_j &= Z_{a,j} - (\mathbf{W}^{Bj})^T \mathbf{u}^B - r_j \\ \dot{g}_j &= \dot{Z}_{a,j} - (\mathbf{W}^{Bj})^T \dot{\mathbf{u}}^B \end{aligned} \tag{9}$$

The superscript $()^T$ denotes the transpose of a matrix. r_j is the road roughness at that point, with respect to displacements, generated as described in Sect. 2.2 with Eq. (16); $Z_{a,j}$ and $\dot{Z}_{a,j}$ are the displacement and the velocity of the j wheel, respectively (Fig. 2). Equation (8) is valid provided the contact force is compressive $\lambda_j > 0$ and the contact distance is zero. When the wheel is detached from the deck, the contact distance is $g_j > 0$ and the normal contact force is equal to zero $\lambda_j = 0$. The re-contact of the wheels to the bridge occurs when $g_j = 0$ and $\dot{g}_j < 0$. Figure 3 illustrates the contact problem for the cases considered in this study: (a) the wheels are in contact with the bridge elements during the analysis ($\lambda_j > 0$), and (b) the wheels separate from the deck ($\lambda_j = 0$ and $g_j > 0$).

With the aid of Eq. (8) the contact force vector becomes:

$$\lambda = \mathbf{K}_c(-\mathbf{W}^T \mathbf{u} + \mathbf{r}_c) - \mathbf{C}_c \mathbf{W}^T \dot{\mathbf{u}} \tag{10}$$

where \mathbf{r}_c is the road roughness function (Zhang and Cai 2011) vector which contains the irregularities of the road surface (Deng and Cai 2010); \mathbf{K}_c and \mathbf{C}_c are simply the *diagonal* matrices of the stiffness and damping parameters of the wheels (Fig. 2):

$$\begin{aligned} \mathbf{K}_c &= \text{diag}\{K_{l1} \ K_{l2} \ K_{l3}\}, \mathbf{C}_c = \text{diag}\{C_{l1} \ C_{l2} \ C_{l3}\} && \text{(3-axle truck)} \\ \mathbf{K}_c &= \text{diag}\{K_{l1} \ K_{l2} \ K_{l3} \ K_{l4} \ K_{l5}\}, \mathbf{C}_c = \text{diag}\{C_{l1} \ C_{l2} \ C_{l3} \ C_{l4} \ C_{l5}\} && \text{(5-axle truck)} \end{aligned} \tag{11}$$

Table 1 Parameters of the vehicle model (see Fig. 2). (Wang et al. 2016; Zhang and Cai 2011; Xu and Guo 2003; Yang et al. 2009)

Parameter	Description	Value (3-axle truck) ^a	Value (5-axle truck) ^b
Mass	1st part of the truck body	2612 kg	9060 kg
	2nd part of the truck body	26,113 kg	29,006 kg
	3rd part of the truck body	–	24,460 kg
	1st axle suspension	980 kg	890 kg
	2nd axle suspension	1616 kg	1780 kg
	3rd axle suspension	1306 kg	1780 kg
	4th axle suspension	–	890 kg
	5th axle suspension	–	1780 kg
Spring stiffness	Upper, 1st axle (K_{u1})	485,208 N/m	791,440 N/m
	Lower, 1st axle (K_{l1})	1,750,164 N/m	3,760,000 N/m
	Upper, 2nd axle (K_{u2})	3,806,344 N/m	5,583,000 N/m
	Lower, 2nd axle (K_{l2})	7006614 N/m	7,520,000 N/m
	Upper, 3rd axle (K_{u3})	3,938,068 N/m	5,583,000 N/m
	Lower, 3rd axle (K_{l3})	7014858 N/m	7,520,000 N/m
	Upper, 4th axle (K_{u4})	–	5,583,000 N/m
	Lower, 4rd axle (K_{l4})	–	3,760,000 N/m
	Upper, 5th axle (K_{u5})	–	5,583,000 N/m
	Lower, 5rd axle (K_{l5})	–	7,520,000 N/m
Damping coefficient	Upper, 1st axle (C_{u1})	4380 N s/m	40,000 N s/m
	Lower, 1st axle (C_{l1})	4000 N s/m	40,000 N s/m
	Upper, 2nd axle (C_{u2})	15,764 N s/m	40,000 N s/m
	Lower, 2nd axle (C_{l2})	4000 N s/m	40,000 N s/m
	Upper, 3rd axle (C_{u3})	14,364 N s/m	40,000 N s/m
	Lower, 3rd axle (C_{l3})	4000 N s/m	40,000 N s/m
	Upper, 4th axle (C_{u4})	–	40,000 N s/m
	Lower, 4th axle (C_{l4})	–	40,000 N s/m
	Upper, 5th axle (C_{u5})	–	40,000 N s/m
	Lower, 5th axle (C_{l5})	–	40,000 N s/m
Length	L_1	4.27 m	1.60 m
	L_2	4.27 m	2.40 m
	L_3	2.22	1.64 m
	L_4	2.34	3.36 m
	L_5	–	2.00 m
	L_6	–	3.06 m
	L_7	–	1.95 m
	L_8	–	2.40 m
	L_9	–	1.64 m
	L_{10}	–	3.36 m
	L_{11}	–	5.06 m
Total truck length	L	13.40 m	16.00 m

^a Zhang and Cai (2011) and Wang et al. (2016)^b Xu and Guo (2003) and Yang et al. (2009)

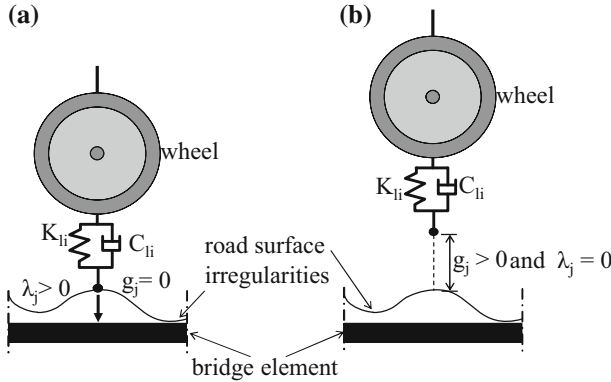


Fig. 3 The proposed approach considers the vertical jumping of the wheels during the SVBI analyses: **a** the wheel is in contact with the bridge element, and **b** the wheel separates from the deck

Substituting the expression of the contact forces vector λ (Eq. (10)) into the equations of motion of the two subsystems [the bridge (Eq. 1) and the vehicle (Eq. 3)], and after some algebra, the equation of motion of the coupled vehicle–bridge system can be cast in the form:

$$M\ddot{\mathbf{u}} + \mathbf{C}^*\dot{\mathbf{u}} + \mathbf{K}^*\mathbf{u} = \mathbf{F}^* \tag{12}$$

where \mathbf{K}^* is the global stiffness matrix, \mathbf{C}^* is the global damping matrix and \mathbf{F}^* is the global force vector:

$$\begin{aligned} \mathbf{K}^* &= \mathbf{K} + \mathbf{W}\mathbf{K}_c\mathbf{W}^T \\ \mathbf{C}^* &= \mathbf{C} + \mathbf{W}\mathbf{C}_c\mathbf{W}^T \\ \mathbf{F}^* &= \mathbf{F} + \mathbf{W}\mathbf{K}_c\mathbf{r}_c \end{aligned} \tag{13}$$

In Eq. (12) \mathbf{M} is the mass matrix, \mathbf{K} is the stiffness matrix and \mathbf{C} is the damping matrix, all created by assembling the pertinent matrices of the two individual subsystems together as:

$$\mathbf{M} = \begin{bmatrix} \mathbf{M}^V & \\ & \mathbf{M}^B \end{bmatrix}, \quad \mathbf{K} = \begin{bmatrix} \mathbf{K}^V & \\ & \mathbf{K}^B \end{bmatrix}, \quad \mathbf{C} = \begin{bmatrix} \mathbf{C}^V & \\ & \mathbf{C}^B \end{bmatrix} \tag{14}$$

Accordingly, the displacement vector \mathbf{u} , the force vector \mathbf{F} and the direction matrix \mathbf{W} are:

$$\mathbf{u} = \begin{bmatrix} \mathbf{u}^V \\ \mathbf{u}^B \end{bmatrix}, \quad \mathbf{F} = \begin{bmatrix} \mathbf{F}^V \\ \mathbf{F}^B \end{bmatrix}, \quad \mathbf{W} = \begin{bmatrix} \mathbf{W}^V \\ -\mathbf{W}^B \end{bmatrix} \tag{15}$$

The coupled equations of motion of the interacting vehicle–bridge system (12) and (13) are numerically integrated in a state-space form with the aid of the available in MATLAB (Mathworks 2012) ordinary differential equation solvers for large, stiff systems.

2.2 Road surface roughness profile simulation

In general, the road surface roughness is an expression of the irregularities of the road surface. The road roughness condition (RRC) affects the dynamic response of both the

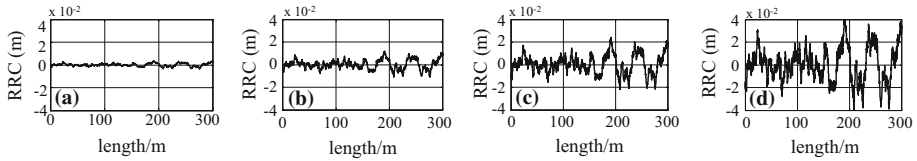


Fig. 4 Samples of Road Roughness profile for **a** ‘very good’, **b** ‘good’, **c** ‘average’, and **d** ‘poor’ conditions, in terms of length per meter

vehicle and the bridge (Deng and Cai 2010; Shi et al. 2008; AASHTO 1996). The road roughness profile is assumed as a zero-mean stationary Gaussian random process and it is generated as an inverse Fourier transform (Wang and Huang 1992),

$$r(x) = \sum_{k=1}^N \sqrt{2\varphi(n_k)\Delta n} \cos(2\pi n_k x + \theta_k) \tag{16}$$

wherein, θ_k is a random phase angle uniformly distributed from 0 to 2π ; n is the spatial frequency; n_k is the wave number (cycle/m); N is the number of frequencies between n_1 and n_2 ; n_1 and n_2 are the lower and upper cutoff frequencies; Δn is the frequency interval between n_1 and n_2 divided by N ; and $\varphi()$ is a power spectral density (PSD) function ($m^3/cycle$) for the road surface elevation. In this study, we use the simplified PSD functions developed by Wang and Huang (1992):

$$\varphi(n) = \varphi(n_0) \left(\frac{n}{n_0}\right)^{-2} \quad (n_1 < n < n_2) \tag{17}$$

where n_0 is the discontinuity frequency of 0.5π (cycle/m); and $\varphi(n_0)$ is the road roughness coefficient ($m^3/cycle$) whose value is chosen depending on the road roughness condition (RRC). The International Standard Organization (1995) provides ranges for the values of RRC according to the road-roughness classification. This study considers from ‘very good’ to ‘poor’ road surface conditions as specified in ISO (1995) (Fig. 4).

3 Case study: modelling and assumptions

This paper presents a direct time-integration dynamic analysis approach for calculating the vertical response of both the vehicle and the bridge of an interacting vehicle–bridge system under seismic excitation.

3.1 The examined bridge

The bridge examined herein (Fig. 1) is an existing R/C highway bridge constructed with the balanced cantilever method. The bridge has a total length of 246.20 m, comprised of three (3) spans with lengths 63.80 m + 118.60 m + 63.80 m. The deck consists of a 14.00 m wide prestressed concrete box girder section. The height of the deck varies from 7.00 m above the piers up to 3.00 m at the midpoint of the middle span and to 2.50 m above the abutments. The structure is supported on two single column piers (P1 and P2) of heights 36.00 and 46.00 m, respectively. The deck is monolithically connected to the piers. Piers have a full height hollow rectangular cross section of 3.50 m × 7.30 m, with 0.74 m

Table 2 Characteristics of the adopted earthquake records. (PEER 2013)

No.	Name	Station	Mag.	Year	Dur. (s)	V_{s30} (m/s)	v.PGA (g)	Sign. dur. (s)	I_A (m/s)
1	Lytle Creek	Wrightwood Park	5.33	1970	16.7	486	0.079	5.285	0.027
2	N. California-07	Cape Mendocino	5.2	1975	14.6	568	0.041	13.695	0.009
3	Oroville-03	Johnson Ranch	4.7	1975	13.3	590	0.073	2.355	0.020
4	Livermore-02	Liv.-Morgan TP	5.42	1980	40.0	551	0.079	20.840	0.003
5	Mammoth Lakes	USC McGee Creek	4.85	1980	22.0	654	0.086	8.185	0.071
6	Almiros	Almiros	5.2	1980	22.6	413	0.085	10.934	0.030
7	Chi-Chi,Taiwan	CHY006	7.62	1999	120	438	0.215	30.132	0.637
8	NW China-03	Jiashi	6.1	1997	15	240	0.384	11.900	0.836
9	Duzce, Turkey	Duzce	7.14	1999	25	281	0.346	10.965	1.131
10	Kocaeli, Turkey	Izmit	7.51	1999	29	811	0.145	16.720	0.350
11	Irpinia, Italy	Sturno	6.9	1980	14.2	382	0.259	9.237	0.490
12	Baja, California	Cero Prieto	5.5	1987	16	471	0.589	3.355	1.922
13	Kobe, Japan	Kakogawa	6.9	1995	41	312	0.158	13.260	0.280
14	Hollister-03	Hollister City Hall	5.14	1974	32	199	0.071	10.390	0.032
15	Irpinia, Italy	Mercato	6.9	1980	42	428	0.054	27.013	0.079
16	Kalamata-01	Kalamata	6.2	1986	19.5	382	0.204	4.992	0.050
17	Kozani, Gr-02	Chromio	5.1	1995	18.3	520	0.072	6.190	0.025
18	Loma Prieta	SF Intern. Airport	6.93	1989	37	190	0.065	16.695	0.059
19	Loma Prieta	Fremont, Mission	6.93	1989	39	367	0.080	18.985	0.120
20	Imperial Val.-08	Westmorland F. St.	5.62	1979	40	194	0.115	10.545	0.007

Mag., moment magnitude of earthquake; Dur., duration of the earthquake; V_{s30} , average shear-wave velocity in the top 30 m of the soil deposit; v. PGA, vertical peak ground acceleration; Sign. Dur., the significant duration of the earthquake excitation; I_A , Arias Intensity of the earthquake

wall thickness. Figure 1 shows the physical model of the selected bridge; the adopted finite element model for the VBI analysis; and the first two modes of the bridge in the vertical direction. For simplicity, the study assumes that the bridge is founded on very stiff soil, hence the piers are effectively fully fixed at their base.

3.2 The assumed vehicle

Under real-life conditions, multiple types of vehicles with different distribution patterns may occupy randomly different lanes, of a highway bridge, at the same time. The vehicle type and the vehicle distribution should be representative of the actual traffic load anticipated. In the absence of real traffic flow information though, the common practice when analyzing the vehicle–bridge interaction, is to use solely one type of vehicle, alone or as a series of identical vehicles (Guo and Xu 2001; Cai and Chen 2004; Chen and Cai 2004). Similarly, the present study assumes that vehicles running on the bridge have the same truck geometry, gross vehicle weight, axle spacing and number of axles. An additional assumption is that the traffic flow is free-flowing and that traffic is only in a single lane of the bridge; this is inevitable since the present approach is two dimensional.

This study utilizes two commonly used types of truck vehicles of Class 8 (CTA 2015). This class of vehicles includes both single-unit trucks (class 8a) and combination of trucks

(class 8b i.e. a truck tractor with one or more trailers) with gross vehicle weight (GVW) above 16.5t.

The first simulated vehicle model (truck A) is the HS20-44 tractor truck with semitrailer (Zhang and Cai 2011), proposed in AASHTO Bridge Design Specifications (1996). It is a three-axle truck (Fig. 2a), with GVW equal to 30t. This type of truck tractor with semi-trailer represents the 75 % of the truck volume on the European roads (Zhou et al. 2015). In addition, it corresponds to the most frequent GVW for loaded trucks (Ghosh et al. 2013). The second vehicle (truck B) is a five-axle truck consisting of a truck tractor connected to two trailers, with GVW equal to 62.5t (Fig. 2b) (Guo and Xu 2001). This truck, is one of the suggested types of trucks to be applied as road traffic actions on bridges in Eurocodes (CEN 1991). Further, truck surveys conducted by Georgia Department of Transportation Highway Performance Monitoring System show that this type of vehicle represents the 65–75 % of the total truck volume of the Interstate truck traffic in the 13 county Atlanta metropolitan area (Ahanotu 1999). These results highlight that truck B is commonly encountered in highway roads. Finally, note that according to the U.S. Department of Transportation (FHWA 2015), the combination-trucks travel, on average, seven times more miles per year compared to single-unit trucks (above 5.0t and having at least six tires) which are typically driven locally.

Concerning the simulation characteristics of the vehicles, the value of stiffness and damping coefficients for tires vary for different types of tires or inflation pressure (Clark 1981). This study uses parameters that have been applied in previous studies for similar types of trucks (Wang et al. 2016; Zhang and Cai 2011; Guo and Xu 2001; Yang et al. 2009). Table 1 lists the main parameters of the two vehicle models used in this study. The reference vehicle speed value is 70 km/h (19.4 m/s) in accordance with the speed limits for

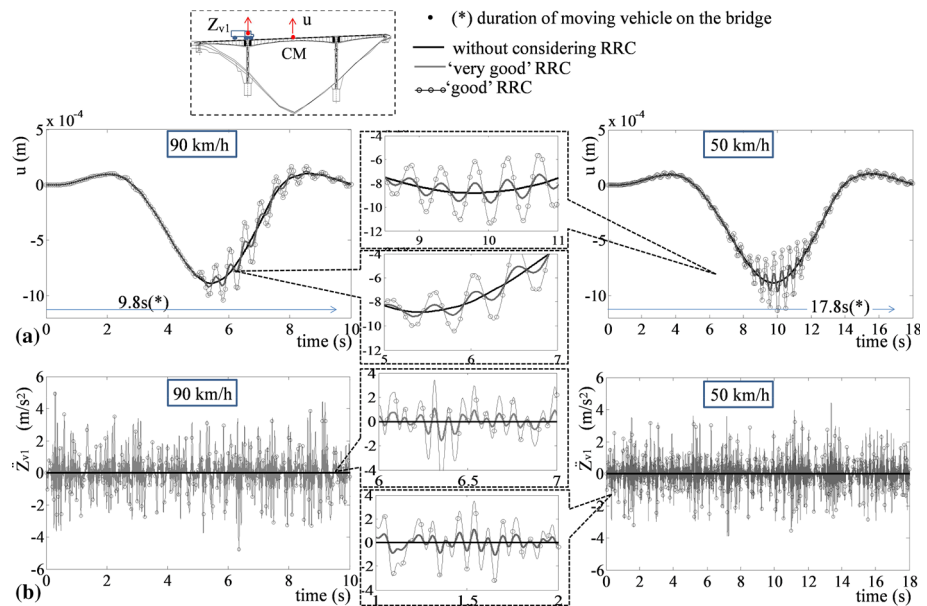


Fig. 5 The effect of road roughness. Response of the vehicle–bridge system in terms of: **a** vertical displacements of the midpoint of the bridge, and **b** vertical accelerations of the truck tractor A, considering various RRCs

heavy trucks (70–80 km/h) worldwide. In addition, vehicle speeds of 90 km/h (25.0 m/s) and 50 km/h (13.8 m/s) are also considered as realistic deviations from the reference value.

3.3 The selected earthquake records

Table 2 summarizes important characteristics of the selected records. The selected group of ground motions includes both moderate and strong earthquake records, corresponding to earthquake events with magnitude between 4.7 and 7.6 (PEER 2013).

4 Seismic vehicle–bridge interaction (SVBI): results

The present section examines the dynamic interaction between moving truck vehicles and a highway bridge during vertical earthquake excitation, with the aid of the proposed approach (SVBI analysis) presented in Sect. 2. Its aim is to bring forward the dominant variables of the problem and their influence on the seismic response of the coupled vehicle–bridge system. A particular goal of this section is to unveil how the seismic response of the bridge affects the running vehicles. In this context, Sects. 4.1 up to 4.4 focus on the acceleration response of vehicles and the deflection of the bridge under moderate (and hence frequent) earthquake excitations, while Sect. 4.5 investigates the detachment (jumping), of the wheels of the truck from the deck of the bridge, including also stronger (and hence less frequent) ground motions.

4.1 The effect of road roughness

In general, the road roughness condition (RRC) affects significantly the vehicle response, and less so, the response of the bridge (Wang and Huang 1992; Xu and Guo 2003; Chen and Cai 2004; Cai and Chen 2004; Zhang and Cai 2011; Zhang and Yuan 2014). Figure 5 illustrates the response of the vehicle–bridge interacting system, for three cases: (1) without considering the RRC (black line), (2) for ‘very good’ RRC (grey line), and (3) for ‘good’ RRC (black line with circles). This section examines a truck A (Fig. 2a) running with (1) 90 km/h (or 25 m/s), and (2) 50 km/h (or 13.8 m/s). The interaction starts when the vehicle enters the bridge and stops when it leaves the bridge. Hence, the total duration the moving vehicle is on the bridge is 9.8 s (for 90 km/h) and 17.8 s (for 50 km/h). As the road roughness condition deteriorates, both the vertical displacements of the bridge and the vertical accelerations of the truck tractor, increase. For lower vehicle speed (50 km/h), the deterioration of the RRC has a stronger effect on the bridge vibration, and becomes noticeable shortly after the vehicle enters the bridge. For 90 km/h, the effect of the road roughness on the response of the bridge is only noticeable after the vehicle passes over the midpoint of the bridge (at $t = 4.9$ s). The peak vertical displacement of the midpoint of the bridge increases by 15 % (for vehicle speed 50 km/h) and 7 % (for 90 km/h) for ‘good’ RRC compared to the corresponding values for ‘very good’ RRC. Similarly, the peak vertical acceleration of the truck tractor is magnified by a factor of 2.5 (for 50 km/h) and 2.7 (for 90 km/h) for ‘very good’ RRC and ‘good’ RRC respectively.

Figure 6 repeats the analyses of Fig. 5, considering the earthquake excitation no. 3 of Table 2. It is assumed that the earthquake strikes when the truck enters the bridge. Overall, for the specific earthquake ground motion (i.e. record no. 3 of Table 2) the effect of the RRC dominates the response of the bridge. Figure 6b illustrates the pertinent seismic

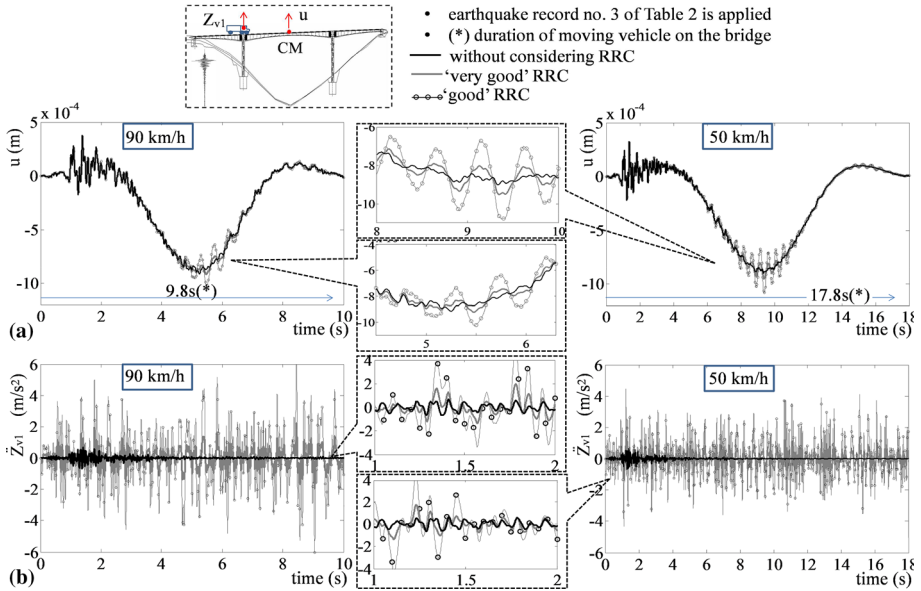


Fig. 6 Seismic response of the vehicle–bridge system in terms of: **a** vertical displacements of the midpoint of the bridge, and **b** vertical accelerations of the truck tractor A, with and without considering RRC and for the ground motion no. 3 of Table 2

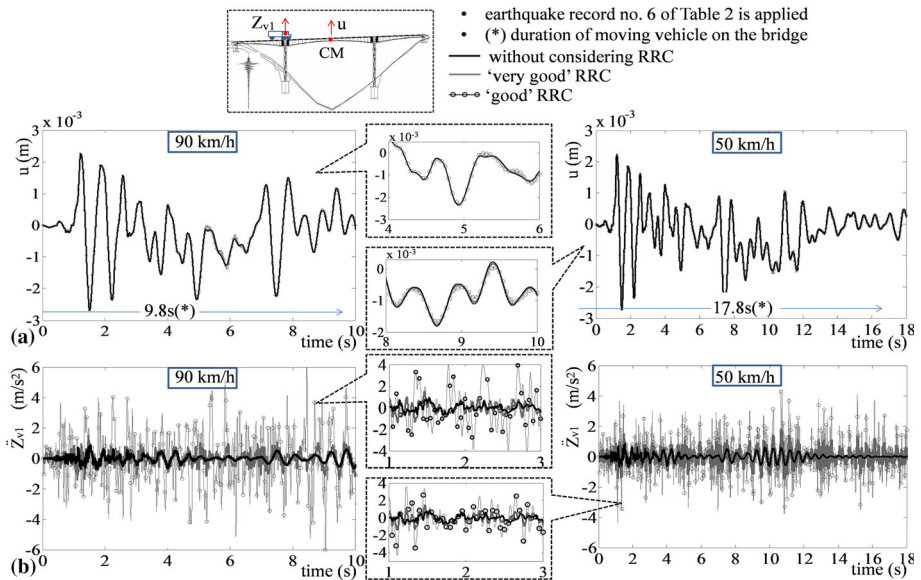


Fig. 7 Same as Fig. 6 for earthquake ground motion no. 6 (Table 2)

response of the vehicle. Note that the analysis accounts for the non-zero starting values of the vertical displacements and the pitching rotations, when the vehicle enters the bridge (time = 0.0 s), due to the deformed configuration of the moving vehicle. As expected, the

deterioration of the road surface quality accentuates the response of the vehicle. The peak vertical accelerations amplify by a factor of 2 for ‘very good’ and by a factor of 6 for ‘good’ RRCs, during the earthquake excitation, respectively. In general, the deterioration

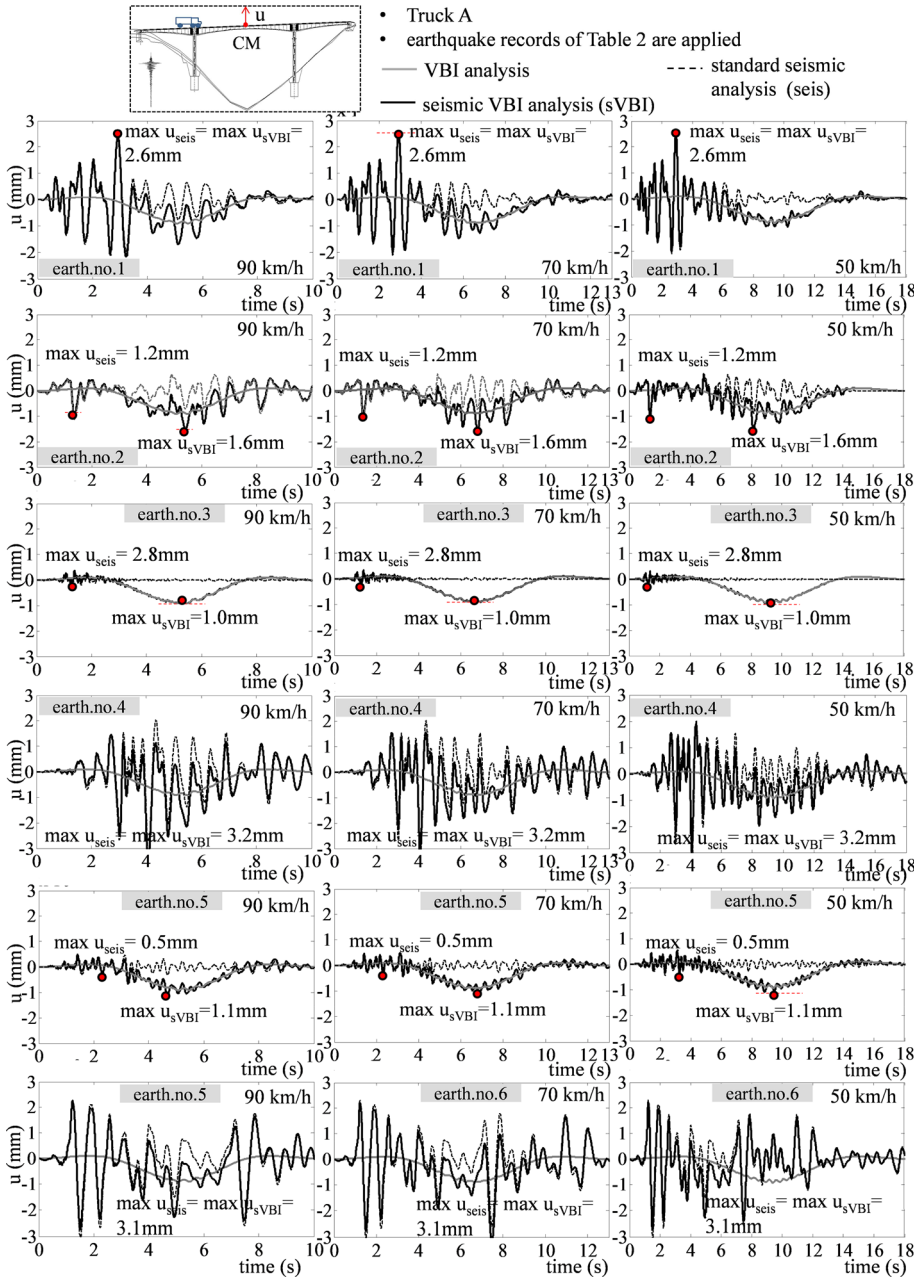


Fig. 8 Vertical displacement time-histories of the midpoint of the bridge, obtained from **a** VBI analyses; **b** seismic VBI analyses; and **c** standard seismic analyses, for various vehicle speeds, and considering truck A

of the RRC combined with the earthquake excitation results in higher vehicle vibration amplitude and becomes more important as the vehicle speed increases (e.g. the peak vertical acceleration appears for the vehicle speed of 90 km/h).

The relative importance of the two sources of excitation, the earthquake ground motion and the RRC, on the response of the VBI system can vary drastically. Figure 7 repeats the analyses of Fig. 6, this time for a ground motion of higher intensity (no. 6 of Table 2). In contrast to Fig. 6 the effect of the RRC is now hardly noticeable on the response of the bridge. The earthquake ground excitation dominates the bridge response while the influence of the RRC becomes secondary. Further, the comparison of Figs. 7a to 6a indicates that when the earthquake has a strong impact on the bridge, the influence of the RRC on the vehicle response is not as important as for earthquakes with lower impact on the bridge. Again, higher vehicle speed results in higher peak values of the seismic response of the vehicle.

4.2 The effect of vehicle speed

This section explores the influence of the vehicle speed on the seismic response of the VBI system, considering one vehicle running with a speed of: (1) 90 km/h (or 25 m/s), (2) 70 km/h (or 19.4 m/s) and (3) 50 km/h (or 13.8 m/s). Figure 8 summarizes the vertical deflections of the midpoint of the bridge for earthquake ground motions no. 1 to 6 of Table 2. It presents three type of analyses: (a) VBI analyses without considering earthquake excitations (grey line); (b) VBI analyses accounting for the earthquake ground motions of Table 2 (continuous black line), henceforth abbreviated as SVBI; and (c) conventional seismic analyses simulating solely the bridge and neglecting the VBI

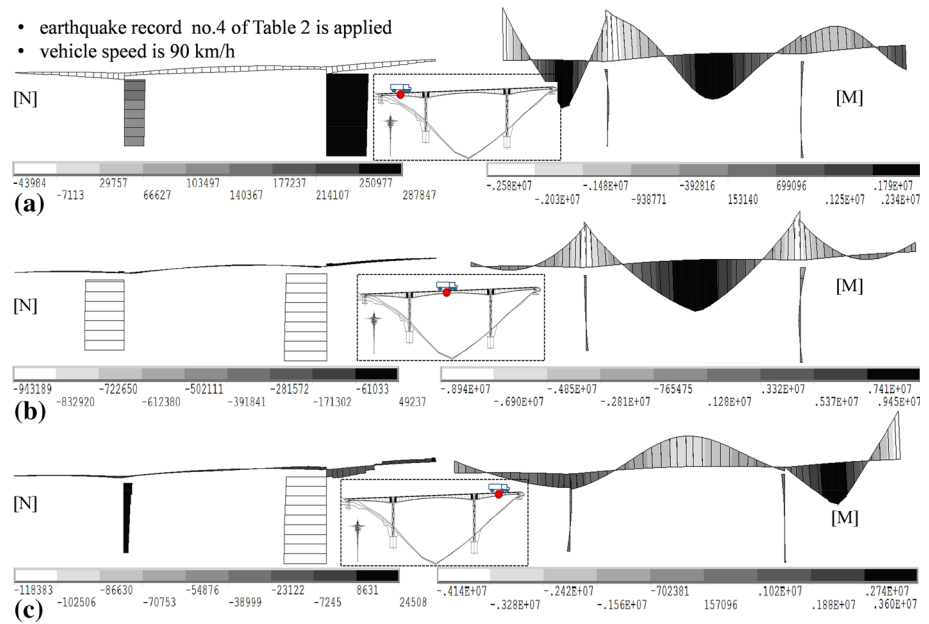


Fig. 9 Axial forces and moments of the bridge, at the time truck A passes over the midpoint of: **a** the first span, **b** the middle span, and **c** the third span. The vehicle speed is 90 km/h

(CEN 2005) (black dashed line). ‘Very good’ RRC are assumed for the VBI and the SVBI analyses (see Fig. 4), and again, for the SVBI analyses (Case b) the earthquake excitation starts at the time instant the vehicle enters the bridge ($t = 0$ s). In general, the vehicle speed might affect differently the seismic response of the bridge. For instance, at a specific time instant of the response, a higher speed can either amplify (i.e. at $t = 5$ s) or de-amplify (i.e. at $t = 12$ s) vertical displacement of the deck. This observation underlines the additional time-speed-dependency complications which emerge from the concurrent action of the seismic and the traffic excitation. The estimated peak vertical displacements of the bridge range for SVBI from 1.1 mm up to 3.2 mm, while for standard seismic analysis from 0.3 mm up to 3.2 mm. For the earthquakes with stronger impact on the bridge (earthquakes no. 1, 4 and 6, in Fig. 8) both the SVBI analyses and the standard study, yield the same peak vertical deck displacements. On the contrary, for ground motions with weaker impact on the bridge (earthquakes no 2, 3 and 5, in Fig. 8), the standard seismic analysis underestimates the peak values of the vertical displacements of the bridge by 85 % up to 72 %. The results for the heavier truck B are similar and are omitted for brevity.

Figures 9 and 10 plot the axial forces and the bending moments of the bridge during the SVBI analysis considering the seismic excitation of no. 4 (Table 2), at the time truck A is passing over the midpoint of: (a) the first span, (b) the middle span, and (c) the last span of the bridge. The vehicle speed is 90 km/h in Fig. 9 is 50 km/h in Fig. 10. All other parameters of the analyses are as in Fig. 8. Note that, even for vehicles being at the same position on the deck the stress in the bridge can be different due to the different vehicle speeds. Again, this is because of the concurrent action of the earthquake ground motion and the traffic excitation and underlines the time-speed dependency of the problem SVBI problem. The case examined is not critical for the seismic design of the piers, since solely the vertical component of the earthquake excitation is considered. However, the SVBI

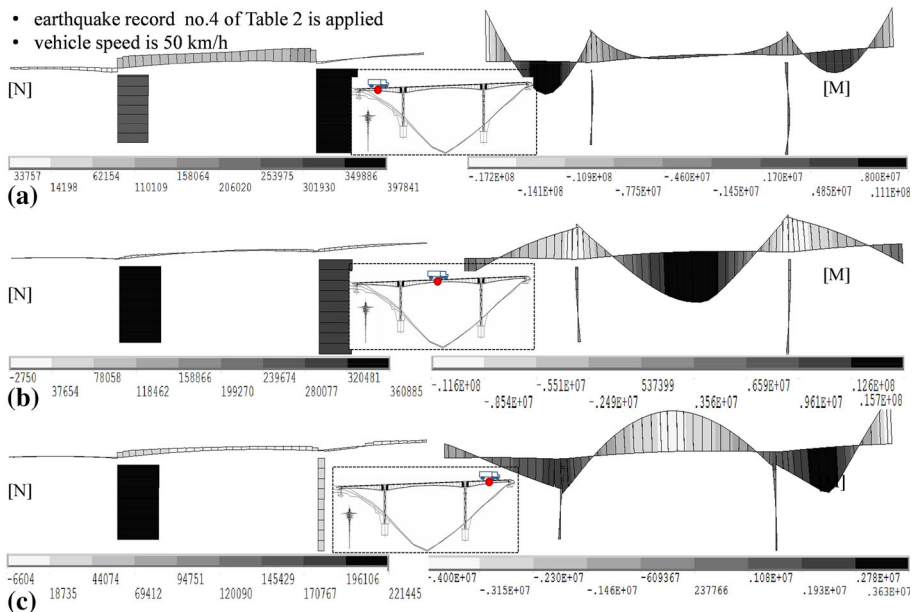


Fig. 10 Same as Fig. 9, but for a vehicle speed of 50 km/h

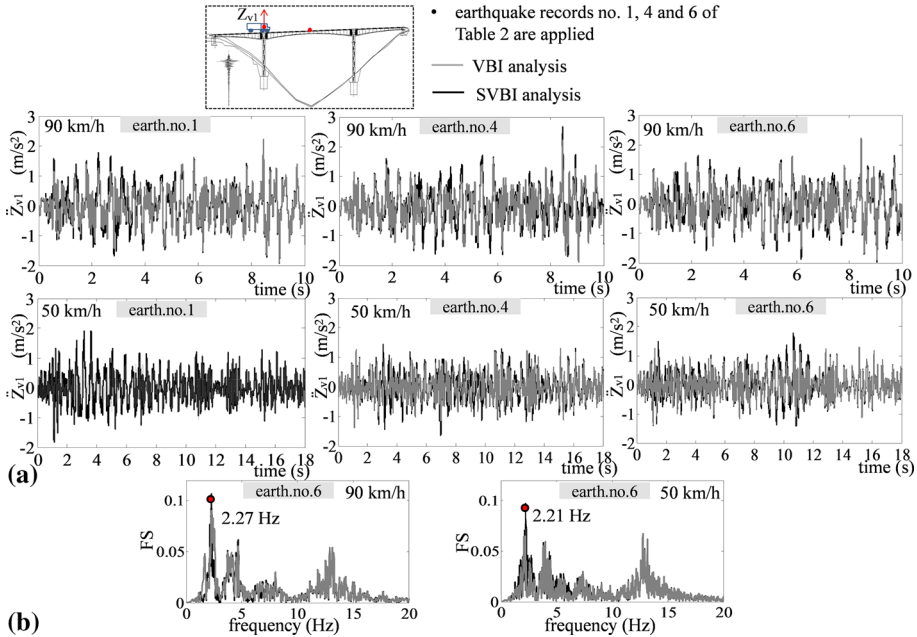


Fig. 11 Response of truck A in terms of vertical accelerations at the truck tractor (a) and two samples of the pertinent Fourier spectra (b), with and without considering earthquake excitations

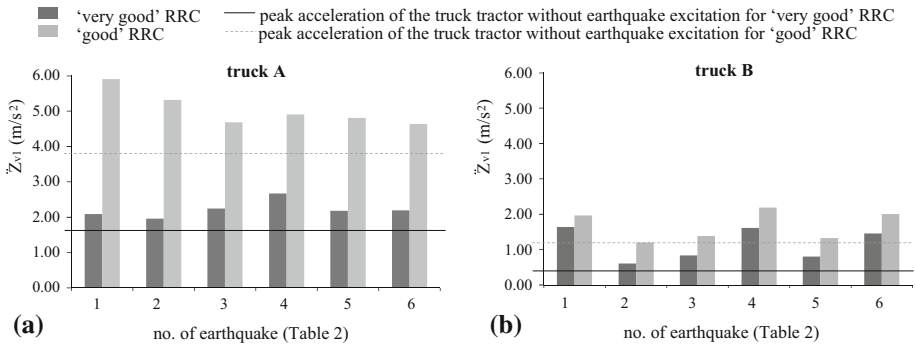


Fig. 12 Peak values of the vertical accelerations of the truck tractor for: **a** truck A and **b** truck B, considering the earthquake ground motions no. 1 up to no. 6 of Table 2 and various RRCs

analysis offers a more realistic view of the stress at (e.g. the midpoint of) the deck which could be critical given that the deck is prestressed.

Figure 11 presents the response vertical accelerations of the truck A tractor, obtained from the VBI analyses of Fig. 8, with (Case b, SVBI analysis) and without (Case a) considering earthquake excitations. Figure 11 plots the results for sample frequent ground motions [no. 1, 4 and 6 (Table 2)] with considerable impact on the response of the vehicle. All the parameters of the analyses are as in Fig. 8. In all cases, the earthquake ground motions amplify the seismic response of the vehicle by a maximum factor of 1.4. Again,

the maximum vertical accelerations appear for the higher vehicle speed (i.e. 90 km/h), for the applied earthquakes. Interestingly, the frequency content of the seismic response of the vehicle is not strongly influenced by the vertical ground motion; see for example the Fourier spectrum of Fig. 11b for ground motion no. 6 of Table 2. This can be attributed to the weak vertical components of the selected ground motions.

Figure 12 illustrates the peak vertical accelerations of the tractors of both trucks (A in Fig. 12a and B in Fig. 12b) for the earthquake excitations no. 1 to 6 of Table 2 and for two different RRCs. The speed of the vehicle is 90 km/h, and it is assumed that the earthquake strikes the VBI system at the time instant the vehicle enters the bridge ($t = 0$ s). For all examined earthquake excitations the peak vertical accelerations of truck A are higher than those of truck B which is attributed to the higher damping values of both the tiers and the suspension system of truck B. Figures 6b, 7b, 11, and 12, also show that for the earthquake ground motions examined (of Table 2) the impact of the road roughness profile is more dominant on the vertical accelerations of the truck tractor, especially when the vertical component of the ground motion is weak (e.g. ground motions no. 2, 3 and 5. of Table 2).

Importantly, for both very good' and 'good' vertical RRC the vertical accelerations of the truck tractor exceed, in all cases, the limits of the vibration comfort given by international experiments on ride comfort (Yang et al. 2009). The acceleration levels are multiple times over the limit of 1.6 m/s^2 which reflects the 'uncomfortable' level of acceptability of ride quality provided by the British Standard Institution (1987). Note however, that the vibration comfort limits refer to the accelerations at the driver's seat, whereas the present results to the accelerations of the truck tractor. Nevertheless, this is an

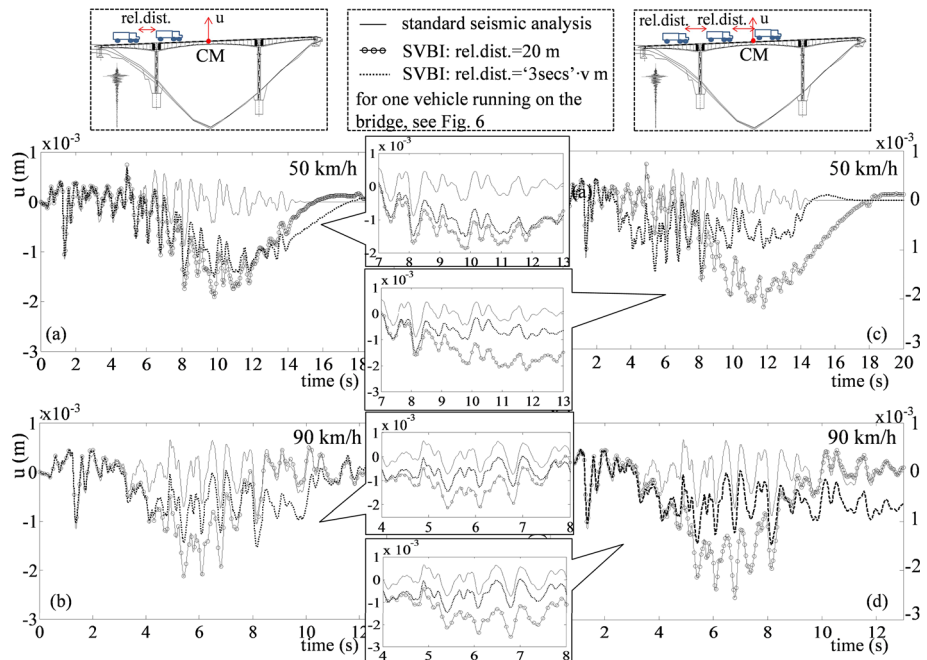


Fig. 13 Seismic response of the midpoint of the deck for: two trucks (left) and three trucks (right) running with different relative distances and constant speeds. Comparison with the corresponding results of the standard seismic analysis

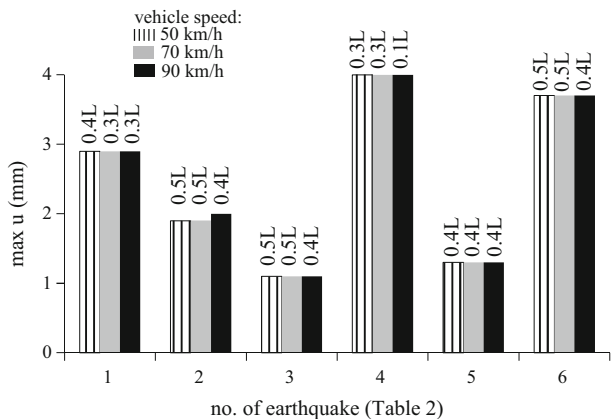
important issue which deserves further research as the excessive vibration of the driver (and the passengers) during earthquake shaking can result in accident. This finding underlines the need for a more detailed study simulating the dynamics of the driver seat in vehicle model (e.g. Yang et al. 2009), in order to obtain more conclusive results regarding the ride comfort during earthquake excitations.

4.3 The effect of the number of vehicles travelling on the deck and of the relative distance between them

Different numbers of vehicles during the earthquake excitation, as well as, different relative distance between them may have important impact on the dynamic vertical response of the bridge. The length of the truck A is 13.40 m. Therefore, a 2 m full-stop bumper-to-bumper minimum gap (Caprani 2012) gives 15.40 m required length for each truck on the deck. Based on this, two different values of relevant distances are examined between the moving vehicles in order to ensure a variety of distances between the moving vehicles: (1) a distance of 20 m, and (2) the “three-seconds rule” distance. The latter is the recommended safe driving distance between vehicles according to the international road safety guidelines (NHTSA 2015). This distance should be increased in adverse weather conditions (e.g. slippery roads or driving at night). Note that, according to the 3 secs rule’, when three vehicles are running along the selected bridge with 25 m/s they cover approximately a total distance of 200 m ($3 \cdot 13.4 + 2 \cdot 3 \cdot 25$).

Figure 13a and b, present the seismic response of the bridge when two type A vehicles are running with constant speeds (50 and 90 km/h, respectively) and different relevant distances: (1) 20 m, and (2) the “3 s rule” distance ($3 \text{ secs} \cdot v$) m on the deck. For all results of Fig. 13, the earthquake ground motion is no. 2 of Table 2, and the interaction starts when the first vehicle enters the bridge and stops when the last vehicle leaves the bridge. The results of the proposed of SVBI are compared with the results from a conventional seismic analysis of the bridge which accounts for the traffic solely as an additional quasi-permanent mass $0.2 \cdot Q_{k,1}$. Figure 13c, d repeat the analyses of Fig. 13a, b for three moving vehicles instead of two. The comparison of all the analyses (Fig. 13a–d), indicates that the peak vertical deflection of the bridge amplifies as the number of vehicles increases and as the relative distance between them decreases. Qualitatively, these results are in agreement with the expected trend based on (static) influence lines. More

Fig. 14 Peak vertical displacements of the midpoint of the bridge, and the corresponding critical positions of truck A on the deck when the earthquake occurs, considering different vehicle speeds



specifically, for 2 vehicles running with a 20 m relative distance and speed 90 km/h, the peak seismic vertical deck displacement is 55 % higher than the pertinent value obtained from the standard seismic analysis. After the first of the vehicles crosses this area, and up to the end of the analyses, the vertical displacements of the bridge increase as the number and the relative distance of the vehicles increase. For this phase of the response, the peak seismic vertical deck deflection is 30 % higher than the pertinent deck displacement of the standard seismic analysis (for 2 vehicles running with a relative distance according to ‘3 secs’ rule and speed 90 km/h).

4.4 The effect of the position of vehicle when the earthquake occurs

So far, all SVBI analyses assume that the earthquake occurs when the (first) vehicle enters the bridge. This assumption though, is arbitrary and it is made solely for the sake of simplicity. The vehicle–bridge–earthquake timing is inherently probabilistic; vehicles can be located at any position on the deck when the earthquake excites the bridge. Yet, their position on the deck during the earthquake shaking influences the seismic response of the interacting vehicle–bridge system.

Figure 14 shows the peak deflections, of the midpoint of the deck, as well as the corresponding locations of truck A on the deck at the instant the earthquake strikes (x/L). It accounts for all three different vehicle speeds, 50, 70 and 90 km/h, assuming ‘good’ RRC in all cases. For most earthquake excitations, the seismic response is accentuated when the vehicle is around the midpoint of the deck (within $0.3\cdot L$ to $0.5\cdot L$) at the time the earthquake occurs. Roughly speaking, when the vehicle is passing over this area of the bridge, at the time the strong ground motion acts, the seismic effects are added on the response of the vehicle–bridge interaction deck and as a result the deck vertical deflections are maximized.

Complementing Figs. 14 and 15 summarizes the peak vertical accelerations of the truck A tractor, for different positions of the vehicle when the earthquake occurs. The speed of the vehicle is 90 km/h (for which the higher peak vertical accelerations of the truck tractor occur), while both ‘very good’ and ‘good’ road roughness conditions (RRC) are examined. All other parameters of the analyses are as in Fig. 14. For all the examined earthquake excitations, the peak vertical accelerations are obtained when the vehicle is located in the region from $0.3\cdot L$ to $0.7\cdot L$ at the time the earthquake occurs. Similarly to the bridge response though, no clear pattern emerges. In conclusion, the influence of the position of

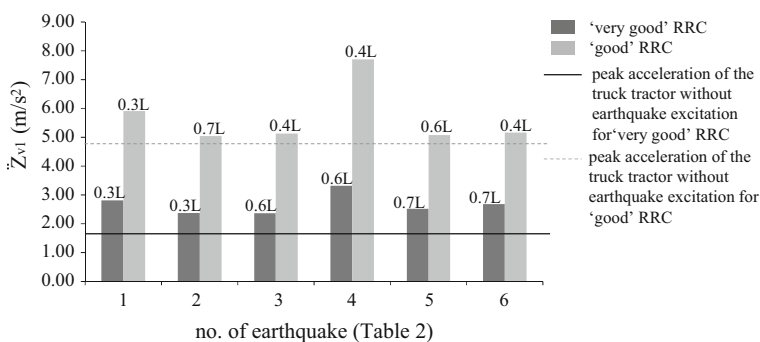


Fig. 15 Peak vertical accelerations of the truck tractor A, and the corresponding position of the vehicle at the time the earthquake occurs. The vehicle speed is 90 km/h

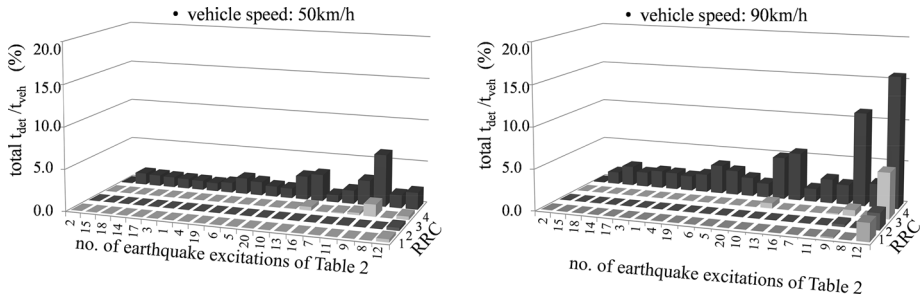


Fig. 16 Total detachment duration as a percentage of the vehicle–bridge interaction duration, for different vehicle speeds and RRCs and vertical earthquake excitations (Table 2) in increasing order of PGA. Truck A is considered

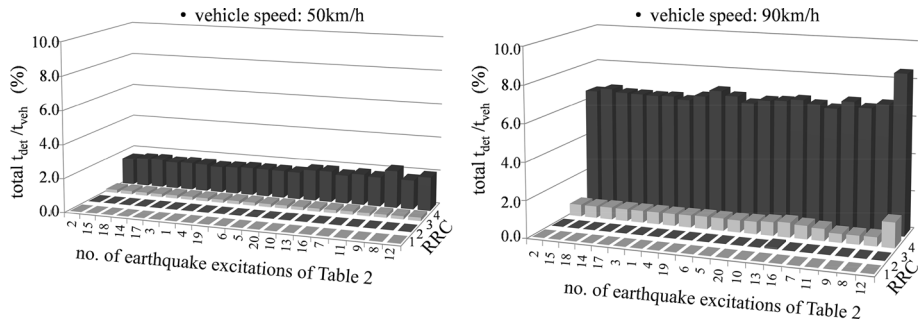


Fig. 17 Same as Fig. 16, considering truck B

the vehicle on the deck at the time the earthquake strikes on the response of the vehicle–bridge system (named herein “vehicle–bridge-earthquake timing” problem) is a multi-parametric and complex problem which beckons for a probabilistic approach in order to obtain conclusions of general value. However, this is beyond the scope of the present study.

4.5 Wheel-deck detachment (jumping)

Beyond the assessment of the vibration levels, another critical issue regarding the safety of the running vehicle is the detachment of the wheels of the truck from the deck during the seismic response of the vehicle–bridge interacting system (see Fig. 3). This section presents the results from SVBI analyses for all the earthquake records of Table 2, considering different RRCs and vehicle speeds. Figure 16 shows the total duration the truck A wheels detach from the bridge as a percentage of the duration of the vehicle–bridge interaction (the vertical axis of the 3-D diagrams). The total detachment time equals the sum of the duration of the individual detachments of all the wheels during the response history. The transverse axis of the 3-D diagram plots different RRCs (‘very good’ RRC 1, ‘good’ RRC 2, ‘average’ RRC 3, and ‘poor’ RRC 4), while the horizontal axis plots the peak ground acceleration (PGA) for all ground motions of Table 2, in increasing order from the

minimum 0.041 g to the maximum 0.59 g value. All other parameters of the analyses are as in Fig. 6.

For the truck A travelling with 90 km/h, no detachment occurs for most of the adopted earthquakes when considering ‘very good’ or ‘good’ RRCs (RRC 1 or RRC 2 in Fig. 16). However, during the earthquake ground motion no. 12, detachment does occur (from 0.2 % up to 1.8 % of the total duration of the moving truck on the bridge). For the same truck and RRCs, running with 50 km/h, detachments of the wheels appear during the same earthquake excitation (i.e. no. 12) but with shorter duration. For both speeds, detachments appear during strong ground motions, with a vertical PGA between 0.16 g to 0.59 g. Assuming ‘poor’ road roughness quality (RRC 4), the wheels of the truck detach from the bridge during all of the adopted earthquake excitations, regardless the vehicle speed. In that case, the duration of the detachments for the strongest adopted earthquake reaches 15.5 % (for 90 km/h).

Similarly, Fig. 17 illustrates the total duration of the wheels of truck B detach from the bridge as a percentage of the duration of the vehicle–bridge interaction (the vertical axis of the 3-D diagrams). All other parameters of the analyses are as in Fig. 16. For truck B travelling with 50 km/h or 90 km/h, when considering ‘very good’ or ‘good’ RRCs, no detachments are observed during the SVBI for any of the examined earthquake excitations. For both speeds, detachment occurs when considering ‘average’ or ‘poor’ road roughness quality, during all the applied ground motions. For the truck running with 50 km/h, the first and fourth axles of the truck detach with an average duration of 1.8 % of the total duration of the moving vehicle (considering ‘poor’ RRC). For the same truck running with 90 km/h, the duration of the detachments increases up to an average value of 6.2 % of the total duration of the moving truck, except of the case of earthquake excitation no. 12 where the percentage increases up to 8.3 %.

Interestingly, even though the total duration of the detachments increases as the PGA of the ground motions increases when truck A travels with 90 km/h, for 50 km/h the longest total detachment duration appears for earthquake excitation no. 9, which is not the vertical ground motion with the highest PGA. Similarly, for truck B traveling with 50 km/h, the longest total detachment duration occurs during the ground motion no. 9, while the total duration of the detachments does not necessarily increase with the increase of the PGA. These observations imply that, for the earthquake excitations applied herein, the detachment of the wheels from the bridge, during the SVBI, depends not only on the PGA of the ground motion but also on its kinematical characteristics and the frequencies of both the moving vehicles and the earthquake excitation of the VBI system.

5 Conclusions

The present study proposes a framework for the seismic response analysis of interacting vehicle–bridge systems during vertical earthquake excitation. Then, it utilizes the proposed framework to conduct a parametric study on a realistic highway (straight R/C) bridge-truck/s case.

The analysis brings forward the two main sources of dynamic excitation, the (vertical) road surface condition and the (vertical) earthquake ground motion, as well as, their relative importance. The road surface condition governs the dynamics of the coupled vehicle–bridge system when the vertical component of the earthquake is weak. For earthquake excitations of higher intensity though, the road roughness becomes immaterial

for the seismic response of the bridge, but it still influences strongly the seismic response of the vehicle. The results also show that, important parameters when analyzing the seismic response of interacting vehicle–bridge systems are traffic variables: the number of moving vehicles, their speed, and the relative distance between. In addition, the parameters of the vehicle models (i.e. stiffness and damping of the tires and the suspension system) also, affect the dynamic response of the VBI system. Further, the position of the moving vehicles on the bridge, at the time the earthquake occurs, influences substantially the seismic response of the vehicle–bridge system. This is an inherently unpredictable “vehicle–bridge-earthquake timing” problem which beckons for a probabilistic treatment.

Finally, the paper examines the tendency of the wheels of both a truck tractor with semitrailer and a truck tractor with two trailers to detach from the deck of the bridge (jump) during earthquake shaking; as expected. For both vehicles examined herein, detachment is more frequent as the road surface condition deteriorates and/or the peak ground acceleration of the vertical ground motion increases. Still, detachment is a complicated phenomenon which depends not only on the intensity but, in addition, on the frequency content and the kinematical characteristics of the ground motion and the frequencies of the bridge and the vehicle and needs further study. Similarly, further research is needed to investigate the seismic response of vehicle–bridge interacting systems in all three spatial dimensions and to account for the non-linear behavior of the bridge and/or the vehicle.

Acknowledgments The authors gratefully acknowledge the Partial Financial support, to the first author, provided by the HKUST Postdoctoral Fellowship Matching Fund.

References

- AASHTO (American Association of State Highway and Transportation Officials) (1996) Standard specifications for highway bridges. AASHTO, Washington
- Ahanotu DN (1999) Heavy-duty vehicle weight and horsepower distributions: measurement of class-specific temporal and spatial variability. Dissertation, Georgia Institute of Technology
- ANSYS (2007) ANSYS User’s Manual, Version 11.0. Swanson Analysis Systems Inc
- Basoz N, Kiremidjian A (1998) Evaluation of bridge damage data from the Loma Prieta and Northridge, California earthquakes. Technical report. Buffalo, NY
- British Standards Institution (BSI) (1987) British Standard Guide to Measurement and Evaluation of Human Exposure to Whole-body Mechanical Vibration and Repeated Shock. BS-6841, BSI, London
- Cai C, Chen S (2004) Framework of vehicle–bridge–wind dynamic analysis. *J Wind Eng Ind Aerodyn* 92(7):579–607. doi:10.1016/j.jweia.2004.03.007
- Caprani CC (2012) Calibration of a congestion load model for highway bridges using traffic microsimulation. *Struct Eng Int* 22(3):342–348. doi:10.2749/101686612X13363869853455
- CEN (European Committee for Standardization) (1991) Actions on structures, Part 2: traffic loads on bridges. Eurocode 1, Brussels
- CEN (European Committee for Standardization) (2005) Design provisions of structures for earthquake resistance—part 2: Bridges. Eurocode 8, Brussels
- Chang SE (2000) Disasters and transport systems: loss, recovery and competition at the Port of Kobe after the 1995 earthquake. *J Transp Geogr* 8(1):53–65. doi:10.1016/S0966-6923(99)00023-X
- Chen S, Cai C (2004) Accident assessment of vehicles on long-span bridges in windy environments. *J Wind Eng Ind Aerodyn* 92(12):991–1024. doi:10.1016/j.jweia.2004.06.002
- Clark SK (1981) Mechanics of pneumatic tires, 2nd edn. U.S. Department of Transportation, National Highway Traffic Safety Administration, S/N 050-003-00377-8
- Cook RD (2007) Concepts and applications of finite element analysis. Wiley, New York
- CTA (Center for Transportation Analysis) (2015) U.S. Department of Energy http://cta.ornl.gov/vtmarketreport/pdf/chapter3_heavy_trucks.pdf. Assessed 18 Nov 2015
- Deng L, Cai C (2010) Development of dynamic impact factor for performance evaluation of existing multi-girder concrete bridges. *Eng Struct* 32(1):21–31. doi:10.1016/j.engstruct.2009.08.013

- Dimitrakopoulos EG, Zeng Q (2015) A three-dimensional dynamic analysis scheme for the interaction between trains and curved railway bridges. *Comput Struct* 149:43–60. doi:[10.1016/j.compstruc.2014.12.002](https://doi.org/10.1016/j.compstruc.2014.12.002)
- Du X, Xu Y, Xia H (2012) Dynamic interaction of bridge–train system under non-uniform seismic ground motion. *Earthq Eng Struct Dyn* 41(1):139–157. doi:[10.1002/eqe.1122](https://doi.org/10.1002/eqe.1122)
- Els P (2005) The applicability of ride comfort standards to off-road vehicles. *J Terramech* 42(1):47–64. doi:[10.1016/j.jterra.2004.08.001](https://doi.org/10.1016/j.jterra.2004.08.001)
- FHWA (Federal Highway Administration) (2015) U.S. Department of Transportation. <http://www.fhwa.dot.gov/policyinformation/statistics/2012/vm1.cfm>. Assessed 20 Nov 2015
- Ghosh J, Caprani CC, Padgett JE (2013) Influence of traffic loading on the seismic reliability assessment of highway bridge structures. *J Bridge Eng*. doi:[10.1061/\(ASCE\)BE.1943-5592.0000535](https://doi.org/10.1061/(ASCE)BE.1943-5592.0000535)
- Guo W, Xu Y (2001) Fully computerized approach to study cable-stayed bridge–vehicle interaction. *J Sound Vib* 248(4):745–761. doi:[10.1006/jsvi.2001.3828](https://doi.org/10.1006/jsvi.2001.3828)
- He X, Kawatani M, Hayashikawa T, Matsumoto T (2011) Numerical analysis on seismic response of Shinkansen bridge-train interaction system under moderate earthquakes. *Earthq Eng Eng Vib* 10(1):85–97. doi:[10.1007/s11803-011-0049-1](https://doi.org/10.1007/s11803-011-0049-1)
- International Organization for Standardization (ISO) (1995) Mechanical vibration-road surface profiles-Reporting of measured data. ISO 8608. Geneva
- Japan Road Association (2002) Design specifications of highway bridges, part V: seismic design. Maruzen, Tokyo
- Kappos AJ, Saiidi MS, Aydinogloy MN, Isakovic T (2012) Seismic design and assessment of bridges: inelastic methods of analysis and case studies, vol 21. Springer, Netherlands
- Kappos AJ, Paraskeva TS, Moschonas IF (2013) Response modification factors for concrete bridges in Europe. *J Bridge Eng*. doi:[10.1061/\(ASCE\)BE.1943-5592.0000487](https://doi.org/10.1061/(ASCE)BE.1943-5592.0000487)
- Kawashima K, Sugita H, Kanoh T (1989) Effect of earthquake on driving of vehicle based on questionnaire survey. *Structural Eng Earthq Eng* 6(2):405s–412s. doi:[10.2208/jscej.1989.410_235](https://doi.org/10.2208/jscej.1989.410_235)
- Kim CW, Kawatani M (2006) Effect of train dynamics on seismic response of steel monorail bridges under moderate ground motion. *Earthq Eng Struct Dyn* 35(10):1225–1245
- Kim C, Kawatani M, Konaka S, Kitaura R (2011) Seismic responses of a highway viaduct considering vehicles of design live load as dynamic system during moderate earthquakes. *Struct Infrastruct Eng* 7(7–8):523–534. doi:[10.1080/15732479.2010.493339](https://doi.org/10.1080/15732479.2010.493339)
- Maruyama Y, Yamazaki F (2002) Seismic response analysis on the stability of running vehicles. *Earthq Eng Struct Dyn* 31(11):1915–1932. doi:[10.1002/eqe.195](https://doi.org/10.1002/eqe.195)
- Maruyama Y, Yamazaki F (2004) Fundamental study on the response characteristics of drivers during an earthquake based on driving simulator experiments. *Earthq Eng Struct Dyn* 33(6):775–792. doi:[10.1002/eqe.378](https://doi.org/10.1002/eqe.378)
- MathWorks (MATLAB) (2012) MATLAB User's guide. The MathWorks Inc., South Natick
- Matsumoto N, Sogabe M, Wakui H, Tanabe M (2004) Running safety analysis of vehicles on structures subjected to earthquake motion. *Q Rep RTRI* 45(3):116–122
- NHTSA (National Highway Traffic Safety Administration) (2015) U.S. Department of Transportation. <http://www.nhtsa.gov/>. Assessed 9 Nov 2015
- PEER (Pacific Earthquake Engineering Research Center) (2013) Ground motion database. <http://ngawest2.berkeley.edu/>. Assessed 9 Nov 2015
- Priestley MJN, Seible F, Calvi GM (1996) Seismic design and retrofit of bridges. Wiley, New York
- Shaban N, Caner A, Yakut A, Askan A, Karimzadeh Naghshineh A, Domanic A, Can G (2015) Vehicle effects on seismic response of a simple-span bridge during shake tests. *Earthq Eng Struct Dyn* 44(6):889–905. doi:[10.1002/eqe.2491](https://doi.org/10.1002/eqe.2491)
- Shi X, Cai C, Chen S (2008) Vehicle induced dynamic behavior of short-span slab bridges considering effect of approach slab condition. *J Bridge Eng*. doi:[10.1061/\(ASCE\)1084-0702\(2008\)13:1\(83\)](https://doi.org/10.1061/(ASCE)1084-0702(2008)13:1(83))
- Tanabe M, Matsumoto N, Wakui H, Sogabe M, Okuda H, Tanabe Y (2008) A simple and efficient numerical method for dynamic interaction analysis of a high-speed train and railway structure during an earthquake. *J Comput Nonlinear Dyn* 3(4):041002. doi:[10.1115/1.2960482](https://doi.org/10.1115/1.2960482)
- Tanabe M, Matsumoto N, Wakui H, Sogabe M (2011a) Simulation of a Shinkansen train on the railway structure during an earthquake. *Japan J Ind Appl Math* 28(1):223–236. doi:[10.1007/s13160-011-0022-4](https://doi.org/10.1007/s13160-011-0022-4)
- Tanabe M, Wakui H, Sogabe M, Matsumoto N, Tanabe Y (2011) An efficient numerical model for dynamic interaction of high speed train and railway structure including post-derailment during an earthquake. In: Proceedings of 8th International Conference on Structural Dynamics EUROODYN. Leuven, Belgium, pp 1217–1223

- Uys PE, Els PS, Thoresson M (2007) Suspension settings for optimal ride comfort of off-road vehicles travelling on roads with different roughness and speeds. *J Terramech* 44(2):163–175. doi:[10.1016/j.jterra.2006.05.002](https://doi.org/10.1016/j.jterra.2006.05.002)
- Wang TL, Huang D (1992) Computer modeling analysis in bridge evaluation. Research report, Florida International University, Department of Civil and Environmental Engineering
- Wang W, Deng L, Shao X (2016) Fatigue design of steel bridges considering the effect of dynamic vehicle loading and overloaded trucks. *J Bridge Eng*. doi:[10.1061/\(ASCE\)BE.1943-5592.0000914](https://doi.org/10.1061/(ASCE)BE.1943-5592.0000914)
- Wibowo H, Sanford D, Buckle I, Sanders D (2012) Effects of live load on seismic response of bridges: a preliminary study. *Civil Eng Dimens* 14(3):166–172. doi:[10.9744/ced.14.3.166-172](https://doi.org/10.9744/ced.14.3.166-172)
- Xia H, Han Y, Zhang N, Guo W (2006) Dynamic analysis of train–bridge system subjected to non-uniform seismic excitations. *Earthq Eng Struct Dyn* 35(12):1563–1579. doi:[10.1002/eqe.594](https://doi.org/10.1002/eqe.594)
- Xu YL, Guo W (2003) Dynamic analysis of coupled road vehicle and cable-stayed bridge systems under turbulent wind. *Eng Struct* 25(4):473–486. doi:[10.1016/S0141-0296\(02\)00188-8](https://doi.org/10.1016/S0141-0296(02)00188-8)
- Yang YB, Wu YS (2002) Dynamic stability of trains moving over bridges shaken by earthquakes. *J Sound Vib* 258(1):65–94. doi:[10.1006/jsvi.2002.5089](https://doi.org/10.1006/jsvi.2002.5089)
- Yang Y, Ren W, Chen L, Jiang M, Yang Y (2009) Study on ride comfort of tractor with tandem suspension based on multi-body system dynamics. *Appl Math Model* 33(1):11–33. doi:[10.1016/j.apm.2007.10.011](https://doi.org/10.1016/j.apm.2007.10.011)
- Yau J (2010) Interaction response of maglev masses moving on a suspended beam shaken by horizontal ground motion. *J Sound Vib* 329(2):171–188. doi:[10.1016/j.jsv.2009.08.038](https://doi.org/10.1016/j.jsv.2009.08.038)
- Zeng Q, Dimitrakopoulos E (2016) Seismic response analysis of an interacting curved bridge–train system under frequent earthquakes. *Earthq Eng Struct Dyn* 45(7):1129–1148. doi:[10.1002/eqe.2699](https://doi.org/10.1002/eqe.2699)
- Zhang W, Cai C (2011) Fatigue reliability assessment for existing bridges considering vehicle speed and road surface conditions. *J Bridge Eng*. doi:[10.1061/\(ASCE\)BE.1943-5592.0000272](https://doi.org/10.1061/(ASCE)BE.1943-5592.0000272)
- Zhang W, Yuan H (2014) Corrosion fatigue effects on life estimation of deteriorated bridges under vehicle impacts. *Eng Struct* 71:128–136. doi:[10.1016/j.engstruct.2014.04.004](https://doi.org/10.1016/j.engstruct.2014.04.004)
- Zhou Xiao-Yi, Treacy Mark, Schmidt Franziska, Brühwiler Eugen, Toutlemonde François, Jacob Bernard (2015) Effect on bridge load effects of vehicle transverse in-lane position: a case study. *J Bridge Eng*. doi:[10.1061/\(ASCE\)BE.1943-5592.0000763](https://doi.org/10.1061/(ASCE)BE.1943-5592.0000763)